A novel lift controller for a wind turbine blade section using an active flow control device including saturations: experimental results

Loïc Michel, Ingrid Neunaber, Rishabh Mishra, Caroline Braud, Franck Plestan, Jean-Pierre Barbot, Pol Hamon

A novel lift controller for a wind turbine blade section using an active flow control device including saturations: experimental results

Loïc Michel, Ingrid Neunaber, Rishabh Mishra, Caroline Braud, Franck Plestan, *Member, IEEE,* Jean-Pierre Barbot, *Senior Member, IEEE,* Pol Hamon

***Abstract*— In this paper, a very recent adaptive version of super-twisting is applied to the control of the aerodynamic lift over wind turbine blades, taking into account local disturbances of the air flow. The proposed control law acts as a model-free control strategy that is based on the definition of only two parameters. Using this strategy, the tuning and modeling efforts are reduced: the first parameter is acting on the gain variation speed, whereas the second one is linked to the expected accuracy, thus allowing the control of unknown dynamics. We discuss the capability of the proposed model to track a lift reference of a wind turbine blade under external perturbations and actuator saturation. Experimental results globally illustrate the feasibility of such a control.**

***Index Terms*— Wind energy, Variable structure systems, Actuators, Adaptive control, Aerodynamics**

I. INTRODUCTION

Wind turbines are subjected to many disturbances (both atmospheric and mechanical) [1], which may, at least on average, be compensated by blade pitch control. Even if the blade pitch control [2] shows global efficiency, it is possible to improve the performances of the closed-loop system by using control scheme acting on aerodynamic variables. Different types of actuation solutions (for example, flaps [3], microtabs [4] or plasma [5]) developed for control purposes, are associated with sufficiently robust control algorithms that are acting on the blade aerodynamics.

A review on the control strategies dedicated to gust alleviation problems using active flow control, is proposed in [6] including modeling techniques [7], [8]. Feedback and feedforward structures [9] have been studied in the framework of a controlled wind turbine blade for active load reduction based on system identification [10] [11] [12] [13] [14].

A proportional controller has been proposed in [15] to reduce lift fluctuations in a constant shear inflow simulated by oscillations of a 2D blade section. Micro-jets have been successfully implemented as a fast control technology and are able to significantly dampen the lift oscillations; however, some lift fluctuations remain. The originality of this work is to control the aerodynamic lift at the blade scale considering active flow control devices (see a review of existing strategies in [16]). The work developed in [15], involving micro-jets, has been improved by using a model-free control technique [17]; this controller has been implemented by the authors [18] to control micro-jets installed at the trailing edge of a 2D blade section. Indeed, it is well-known that modelling and simulation of aerodynamic dynamics are very complex and take a lot of computation time. Consequently, it is difficult to use model for control design.

Afterwards, two ways to design a control of an aerodynamics system are to build an approximated model that is dedicated to control, or to design a control algorithm without needing a model. In [19], several model-free controllers are presented and the advantages of such approach are highlighted. Thus, in [18], a model-free control based on the seminal work [17] is experimented for the blade lift control. The main advantage of this control law is obviously the reduced knowledge with respect to the dynamic of the system; however, it does not offer any guarantee on stability and robustness. It is why, in this work, another class of control, sliding mode control (SMC) [20] [21], requesting few information with respect to the dynamic, is proposed. This control law is a robust nonlinear one with respected to matching perturbation [22] that is particularly well suited to control perturbed uncertain nonlinear systems. Remark that the sliding mode control requests the knowledge of the input-output sign, the relative degree of the system and the boundness of functions describing the dynamic of the system (remark that this latter point is not required in [17]).

Extremum-seeking control (ESC), associated with sliding mode control [20] [21], has been implemented in the framework of aerodynamic drag reduction [23]. The ESC method has also been used as a real-time optimization strategy to cope with high-lift problems in the context of flow instability at the blade section scale through active flow control [24]. However, due to its discontinuous feature, this class of control strategy generates the chattering phenomenon (high frequency oscillations). Several solutions have been proposed to attenuate this drawback; among them, one can firstly cite the concept of high order sliding mode control. This class of controllers allows to reduce the chattering while keeping the robustness and improving the accuracy. One of the most famous high

L. Michel, F. Plestan, J.-P. Barbot and P. Hamon are with Nantes Université, Ecole Centrale Nantes, CNRS, LS2N, UMR 6004, F-44000 Nantes, France. **Corresponding author**: Loïc Michel, loic.michel@ec-nantes.fr.

I. Neunaber, R. Mishra and C. Braud are with Nantes Université, Ecole Centrale Nantes, CNRS, LHEEA, UMR 6598, F-44000 Nantes, France.

J.-P. Barbot is also with ENSEA, Quartz Laboratory, EA 7393, F-95014, Cergy-Pontoise, France.

P. Hamon is also with ARMOR MECA Développement, F-22490, Pleslin-Trigavou, France.

A preliminary version has been published in IEEE Conference on Control Technology and Applications CCTA, Trieste, Italy.

order sliding mode controllers is the super-twisting [25] that is a second order sliding mode algorithm that is a continuous output feedback.

Another way to reduce the chattering is the dynamic adaptation of the controller gain: the simple idea is to adapt the controller gain with respect to the accuracy (the gain is increased if the accuracy is not sufficient whereas, when the targeted accuracy is reached, the gain is reduced). Numerous adaptation laws have been proposed for first [26], [27], [28], [29], [30], [31] or second order sliding mode controllers such as twisting [32], [33], [34] or super-twisting [35], [36], [37], [38].

In this paper, the choice towards the adaptive super-twisting algorithm has been made for several reasons: this is a continuous controller that does not use the time derivative of the sliding variable while reducing the chattering efficiently and the effort of the actuator. Furthermore, there exist several adaptive versions of super-twisting, from the initial version [35] to very recent ones [39], [40], these latter using very few tuning parameters (in [40], [39], two parameters when six for [35]). Notice that this class of adaptive controllers requires a very reduced knowledge of the system; only the facts that the uncertainties/perturbations are bounded and that the system can be modelled as a first order model, are required.

For the first time in aerodynamics, the adaptive super-twisting algorithm, proposed in [40] and based on authors previous work [41], is implemented to control the lift using micro-jets; only global aerodynamic force measurement is used as a feedback for the control. The physical limitation of the actuator will be also taken into account by means of an associated anti-windup algorithm. Its purpose is to maintain the stability of the adaptation procedure of the proposed algorithm in presence of external perturbations that induce actuator saturation.

The paper is structured as follows. Section II describes the experimental setup, whereas Section III presents the adaptive super-twisting algorithm including its main properties and the proposed anti-windup algorithm. Section IV illustrates and analyses some experimental results. Section V gives some concluding remarks and perspectives.

II. Experimental setup

The experimental bench, detailed in this section, is composed of a wind tunnel with its perturbation system, a 2D aerodynamic blade profile equipped by micro-jets (for the lift control), and lift and drag sensors.

A. Wind tunnel facility and gust generator

The LHEEA aerodynamic wind tunnel is a recirculating one. The test section has a cross-section of $500 \times 500\,\mathrm{mm}^2$ and a length of 2300 mm (Figure 1). The turbulence intensity of an undisturbed inflow in the wind tunnel is around 0.3%. In the present study, a grid is installed at the inlet of the test section to generate turbulent inflow with a turbulence intensity of 3%. This bypasses the laminar-to-turbulent transition occurring at low Reynolds numbers and low angles of attack (AoA) for this blade geometry (see the linear part of the lift curve in Figure 2). The inlet of the test section is additionally equipped with a system which enables the generation of a sudden variation

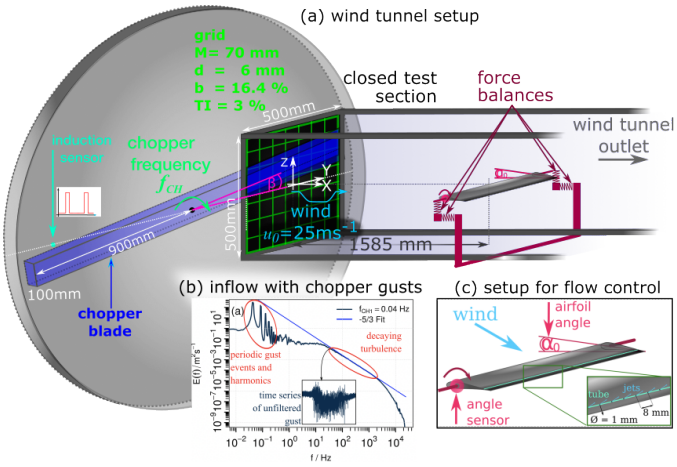

Fig. 1: (a) LHEEA aerodynamic wind tunnel: a gust generator, named “chopper”, can optionally be used. (b) Example of the energy spectrum of the flow generated by the chopper. (c) Setup used for active flow control measurements: a tube with holes is installed at the airfoil’s trailing edge and pressurized air is blown out of the holes.

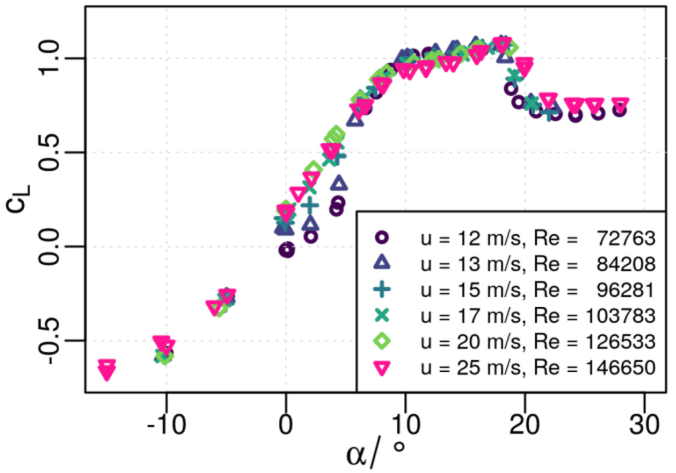

Fig. 2: Experimentally measured lift curves, C_L, versus the angle of incidence, α, of the airfoil in dependence of the Reynolds number.

of the mean flow with turbulence superimposed on it. This system is called ”chopper” and consists of a rotating bar that cuts through the inlet of the test section (Figure 1(a)). Figure 1(b) displays the energy spectrum of a gust produced by the chopper. In this work, however, the chopper is used in a static way by fixing its position in the inlet to add disturbances (in [18], the rotating chopper was used to produce a periodic reduction of the lift).

B. Aerodynamic profile

A 2D blade section of type NACA $65_4 - 421$ with a chord length of $c = 9.6$ cm is installed in the test section

of the wind tunnel (Figure 5).[1] It is a thick profile with two changes of the lift curve corresponding to a first boundary layer separation at the trailing edge of the profile and a second flow separation at the leading edge, indicating stall (see [42] for more details on the blade aerodynamics). In the present study, the angle of incidence was set to $\alpha = 20°$. Open-loop tests for $\alpha = \{0°, 10°, 20°\}$ have been performed to chose this value (see Fig. 3). It has been shown that only a low range of the lift variation (or controlability margin of the lift) can be reached for $\alpha = 0°$ when the flow is still attached (*i.e.* maximum lift force gain $\Delta F_L = 2.5\,\text{N}$). At $\alpha = 10°$, the controlability margin is three times higher ($\Delta F_L = 7\text{N}$), but it is decreasing with the inlet pressure from $p = 1\,\text{bar}$. An angle $\alpha = 20°$ is therefore chosen to operate the control algorithm, as the controlability margin is higher and linearly increasing according to the inlet pressure. More investigations are needed to extend the present work to other angles of incidence.

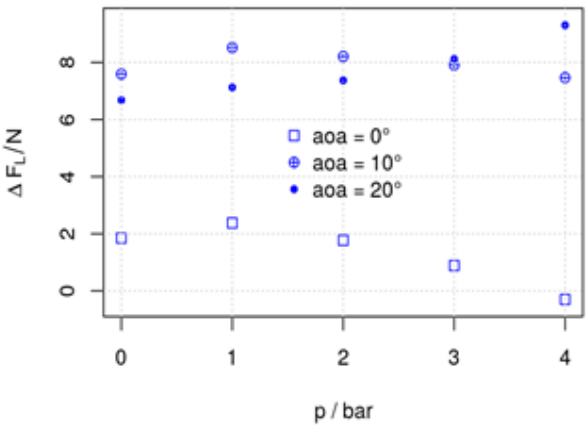

Fig. 3: Lift force gain, ΔF_L, versus pressure for different AoA.

C. Lift and drag measurements

Two sets of Z6FC3 HBM bending beam load cell sensors are used, and they are mounted on both sides of the 2D blade section support to measure the lift and drag forces. As shown in Figure 1(a), each set consists of two load cells mounted with in a 90° angle to measure the forces in the X (drag) and Z (lift) directions. They are calibrated *in situ* using gauge weights from $0 - 5\,\text{kg}$ in steps of $0.5\,\text{kg}$.

D. Micro-jets

To control the flow around the airfoil, holes of 1 mm diameter with equidistant 8 mm spacing are placed at 1.92 cm from the airfoil's trailing edge, along the entire spanwise direction (Figure 1(c)). They are connected to a plenum chamber, itself fed with pressurized air at 6 bar. The air circuit is connected to solenoid valves that are acting as On/Off switches, so that pulsed micro-jets can be generated with a repetition rate of up to 300 Hz.

The action of the micro-jets is physically limited to the injection of pressurized air of maximum 6 bar, thus defining the range of the lift variations that can be compensated by the micro-jets actuator system. It is identified by a simple succession of valves opening and closing.

E. Control hardware

The control is managed by a STM32 Nucleo board H743ZI2 allowing a 16-bit ADC acquisition as well as the possibility to monitor the signals in real-time on the computer (Figure 4 presents the control hardware where the Nucleo board is mounted on a fully featured PCB): the lift force measured by the force balances is used as input signal. It is acquired with a sampling frequency of 20 kHz using the Nucleo board. The signal is filtered using a fourth order Butterworth filter with a cut-off frequency of 20 Hz. The control updates at 20 kHz and drives the duty-cycle of the activation of the valve at 200 Hz in response to the input from the load cell sensors.

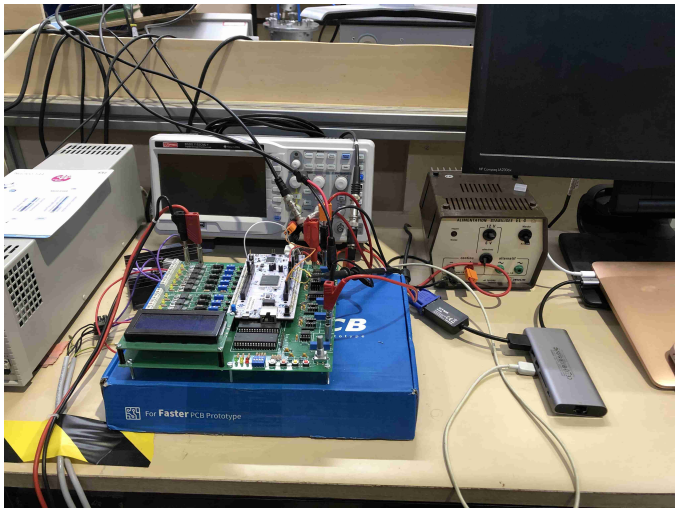

Fig. 4: Experimental setup: the board control.

Figure 5 displays a view of the experimental setup focusing on the wind tunnel, the measurement system and the air injection system.

III. Adaptive super-twisting based controller design

A. Problem statement

The control objective is to ensure that the lift of the blade is tracking a reference despite the wind variations and external perturbations. This is achieved using the action of the micro-jets. As shown in Fig. 6, the control signal drives the signal sent to the solenoid valves to release or block the pressurized air in front of the micro-jets on the airfoil surface. The measured lift is forced to a reference and the valve is driven using a variable duty-cycle (conversion of the output of the control as a PWM signal with a resolution of 0.025 % of the sampling period) at the constant frequency of 200 Hz,

[1]Note that "2D blade section" here refers to a two-dimensional shape that is extruded in the third dimension so that the blade section spans the whole length of the wind tunnel.

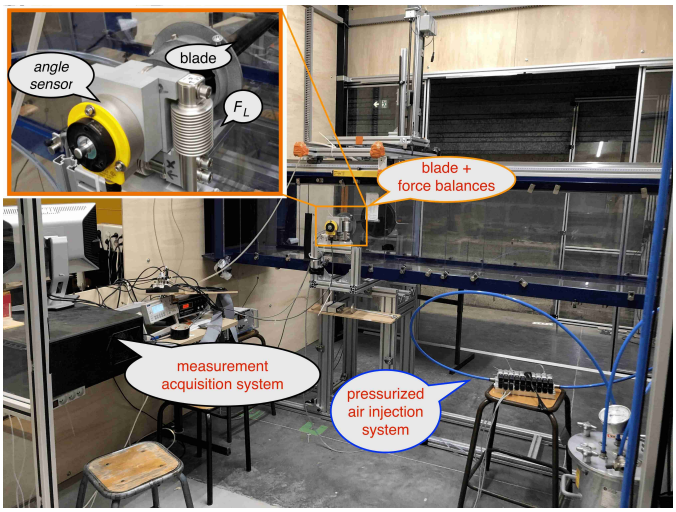

Fig. 5: Experimental setup: the wind tunnel test section with the 2D blade section, load cell sensors, measurement acquisition, and pressurized air injection system.

which is a TTL (transistor-transistor logic) signal. This allows to directly drive the valves from the control signal that adjusts the mass flow injected to the system. Recall that the flow injected at the top of the blade can be not at all sufficient to compensate strong lift variations, therefore inducing saturation of the actuators, that are managed by a anti-windup algorithm.

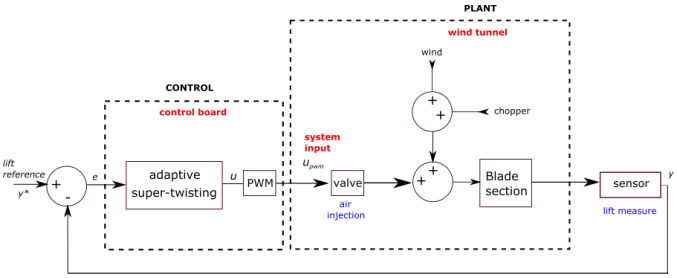

Fig. 6: Closed-loop scheme.

B. A solution with limited knowledge of the system

The blade lift control design is based on the following observation: the modeling of the studied system is a very hard task. Thus, a control approach with a limited modeling process is considered. In such way, the model-free controller [17] has been proposed in [18]: it is assumed that the relation between the force generated by the micro-jets and the lift force (see Figure 6) can be modelled by a first-order system. However, the robustness of such a controller is not ensured. The current paper proposes an adaptive robust controller based on a second order sliding mode strategy [20] that is based on an adaptive version of the super-twisting algorithm [40] given that

- it can be applied to a system with a relative degree equal to 1: that is the case here given that, as shown in [18], the system can be viewed as a first-order system;
- it does not require any modeling information (except the relative degree), its gain being dynamically adapted;
- it is intrinsically robust with respect to uncertainties and perturbations. Indeed, in such conditions, a real second order sliding mode [20] is established in finite time.

Define the tracking error as σ such that $\sigma = y - y^*$ with y the measured lift and y^* the reference. The relation between σ and the control input u that is applied to the PWM system controlling the servo-valves, can be viewed as a perturbed first-order system with unknown static gain k and constant time τ under a perturbation $\delta(t)$ [18], that is

$$\dot{\sigma} = -\frac{1}{\tau}\sigma + \frac{k}{\tau}u + \delta(t). \tag{1}$$

Supposing that parameters k and τ are constant but unknown, system (1) can be written as

$$\dot{\sigma} = a(\sigma, t) + b \cdot u \tag{2}$$

with $a(\sigma,t) = -\frac{1}{\tau}\sigma + \delta(t)$ and $b = \frac{k}{\tau}$. One supposes that the function $a(\sigma,t)$ is bounded in the operating domain. Notice that, in sliding mode context, the variable σ is called "sliding variable". Moreover, $-\frac{1}{\tau}\sigma$ is a dissipative term that contributes to the boundedness of $a(\sigma,t)$.
Given that b is assumed to be constant (but unknown), system (2) has a similar form than the systems considered in [40]. From [40], the adaptive super-twisting controller is defined as

$$\begin{aligned} u &= -k_1 \left|\sigma\right|^{\frac{1}{2}} \mathrm{sgn}(\sigma) + v, \\ \dot{v} &= -k_2 \,\mathrm{sgn}(\sigma). \end{aligned} \tag{3}$$

where u is the output of the controller and the adaptive gains k_1 and k_2 obtained by

$$\dot{k}_1 = \begin{cases} \dfrac{\beta}{|\psi| + \epsilon} & \text{if} \quad |\sigma| > \epsilon \\ -k_1 & \text{if} \quad |\sigma| \leq \epsilon \end{cases} \tag{4}$$

$$\dot{k}_2 = \begin{cases} \dfrac{\beta}{2|\sigma|^{\frac{1}{2}}} & \text{if} \quad |\sigma| > \epsilon \\ -k_2 & \text{if} \quad |\sigma| \leq \epsilon \end{cases} \tag{5}$$

where $\psi = -\hat{\dot{\sigma}}$, $\beta > 0$ and $\epsilon > 0$ are constant parameters; $\hat{\dot{\sigma}}$ is the numerical estimation of $\dot{\sigma}$. For the sake of implementation simplicity, the numerical estimation of $\hat{\dot{\sigma}}$ is performed using the basic Euler method [43][2].

The gains k_1 and k_2 are adjusted based on the proposed adaptation laws (4)-(5). The adaptation protocol drives the evolution of the gains k_1 and k_2 according to the value of σ. The main ideas behind the adaptation rules are the following

- if $|\sigma| > \epsilon$, it can be due to the fact that the gains are not sufficient with respect to the effects of the perturbations and uncertainties (recall that a and b in (2) are unknown, a being bound and b constant). So, the gains are increased (as displayed by first equations (4)-(5)) as long as the

[2]Notice that other estimation techniques could be used, for example based on algebraic technique [44] or homogeneous one [45]. A comparison between different differentiators can be found in [46] as well as discrete time differentiator based sliding modes with polynomial corrector terms with respect to the sampling period [47] and differentiators with variable exponent to improve the rejection of the noise [48].

desired accuracy is achieved, the parameter ϵ adjusting this accuracy target;
- if $|\sigma| < \epsilon$, the accuracy target is reached. The gains can be assumed to be sufficient with respect to the perturbations and uncertainties. In that manner, the gains can be reduced as displayed by the gain dynamics (second equations of (4)-(5)). When the gains become too small or if a larger perturbation/uncertainty appears, the accuracy can be lost; the previous item is then considered, and so on.

Since the convergence zone depends on the parameter ϵ, it is necessary to chose it sufficiently small to ensure the accuracy of the closed-loop system; however, it is necessary to tune it at a sufficient value in order to take into account the sampling period effect (see Section 4 of [26] for the relation between the accuracy target ϵ and the sampling period). The parameter β is acting on the dynamics of adaptive gains and should be chosen according to an initial estimation of the "magnitude" of the open-loop dynamic response of the system including an estimation of the perturbation[3].

C. Saturated actuator

To deal with the physical limits of the micro-jet actuator, that may create uncontrollable situations and unexpected behavior of the control algorithm, in presence of strong perturbations of the lift, an anti-windup procedure [49] is proposed to manage the integration part of the adaptive super-twisting algorithm when physical saturation occurs. Here, only upper saturation is considered due to physical limitations of the experimental test-bench.

1) Definition of the saturation: The control is affected by a saturation including an hysteresis and an anti-windup algorithm that interacts with the numerical integration schemes of the controller. Denoting u the output of the control law, u_{out} the output of the saturation and u_{max} the upper bound of the saturation, the saturation including an hysteresis is defined as follows

- when u increases and $u \geq u_{max}$, then $u_{out} = u_{max}$;
- when u decreases and $u < 0.9\, u_{max}$ then $u_{out} = u$;
- when u remains below u_{max}, then $u_{out} = u$.

2) Anti-windup algorithm: Consider the three numerical integrators, $v_n, k_{1,n}, k_{2,n}$ and their respective derivatives $\dot{v}_n, \dot{k}_{1,n}, \dot{k}_{2,n}$, associated with an anti-windup based integration scheme

$$\begin{aligned} v_n &= v_{n-1} + (1-AW)\frac{h}{2}(\dot{v}_n + \dot{v}_{n-1}) \\ k_{1,n} &= k_{1,n-1} + (1-AW)\frac{h}{2}(\dot{k}_{1,n} + \dot{k}_{1,n-1}) \\ k_{2,n} &= k_{2,n-1} + (1-AW)\frac{h}{2}(\dot{k}_{2,n} + \dot{k}_{2,n-1}) \end{aligned} \tag{6}$$

where n is the discrete time iteration and AW is the variable associated to the anti-windup scheme, that is enabled when entering into the saturation mode. Using Euler numerical differentiation, equation (6) becomes

$$\begin{aligned} v_n &= v_{n-1} + \frac{1}{2}(1-AW)(v_n + v_{n-2}) \\ k_{1,n} &= k_{1,n-1} + \frac{1}{2}(1-AW)(k_{1,n} + k_{1,n-2}) \\ k_{2,n} &= k_{2,n-1} + \frac{1}{2}(1-AW)(k_{2,_n} + k_{2,n-2}) \end{aligned} \tag{7}$$

which is now independent from the time derivative variables $(\dot{v}_n, \dot{k}_{1,n}, \dot{k}_{2,n})$.

Before entering into the saturation mode, the anti-windup scheme is disabled ($AW = 0$) and the integration operates normally.

Entering into saturation mode and assuming that u enters into saturation at the instant $n_{\mathbf{in}}^{sat}$, the anti-windup scheme is enable ($AW = 1$) thus blocking all integrators to their previous values at the instant $n_{\mathbf{in}}^{sat}$. The integrators read

$$\begin{aligned} v_n &= v_{n_{\mathbf{in}}^{sat}} \\ k_{1,n} &= k_{1,n_{\mathbf{in}}^{sat}} \\ k_{2,n} &= k_{2,n_{\mathbf{in}}^{sat}} \end{aligned} \tag{8}$$

Note that the control (3) is still updated during the saturation mode, holding k_1, k_2 and v constant.

Exiting the saturation mode and assuming that u exits out of the saturation at the instant $n_{\mathbf{out}}^{sat}$, the integrators are re-enabled from their prior values (8).

We would like to remark that it is possible to add a scaling coefficient γ on v in order to accelerate the transient response of v at the end of the saturation so that

$$v_{n_{\mathbf{out}}^{sat}} = \gamma\, v_{n_{\mathbf{in}}^{sat}}, \tag{9}$$

From a practical point of view, setting $\gamma < 1$ allows to accelerate the saturation output, and thus to minimize the associated delay but to the detriment of a less efficient tracking.

IV. Experimental results

A. Scenarios of operation

The experiments are conducted considering a constant inflow velocity of 20.3 ms^{-1} (except for scenario 7 which is using an inflow velocity of 19.3 ms^{-1}), measured with a Pitot tube in front of the airfoil in the undisturbed flow, and an angle of incidence of the 2D blade section of 20°. The chopper can create a reduction of the air flow and is used to evaluate the robustness of the proposed adaptive super-twisting control under perturbations of the lift.

The efficiency of the lift tracking is evaluated for several scenarios that illustrate several operating conditions, including change of the wind speed, introduction of the chopper perturbation, and several types of references, for which the characteristics are summarized in the Table I.

To illustrate the operation of the saturation mode, a higher output reference than the maximum reachable lift is considered in order to saturate the micro-jet actuator in the yellow scenarios of Table I.

[3]Notice that current works are made in order to remove the tuning process of ϵ and β, by using an online tuning process of both these parameters.

sc. #	type of reference			type of perturbation	
	Cte	sine	piece-wise	wind speed	chopper
1			X		X
2			X	X	X
3		X			
4	X				X
5			X		X
6			X		X
7			X	X	

TABLE I: Overview of scenarios of operation.

Concerning the scenario 1 and 2, the parameters of the adaptive super-twisting controller are set to $\beta = 7000, \epsilon = 0.1$ and the initial values of both gains are $k_1(0) = k_2(0) = 10$ Concerning the scenarios 3-7, the parameters are set to $\beta = 15000, \epsilon = 20$ and the initial values of both gains are $k_1(0) = 10$, $k_2(0) = 300$. Note that in the different studied cases, with respect to such kind of active flow control, the range of β (resp. ϵ) is between 5000 and 8000 (resp. 0.05 and 0.5) concerning the scenario 1 and 2 and the range of β (resp. ϵ) is between 13000 and 18000 (resp. 10 and 30) concerning the scenarios 3-7.

B. Results and discussion

In each scenario developed below, the tracking of the instantaneous lift is presented according to the time evolution of the duty-cycle and the time evolution of the gains k_1 and k_2.

Scenarios without saturation:

- **Scenario 1:** Figure 7 illustrates the open-loop behavior of the lift force without air injection before introduction of the closed-loop control. The control tracks the reference considering piece-wisely constant changes of the reference. The introduction of the chopper in the test section during the whole scenario is considered. The wind speed is initially set to 20.3 ms^{-1}. Using a fixed position of the chopper blade, a perturbation is introduced at the beginning of the test to set the 'nominal' lift value in the open-loop. Then, the control starts at $t = 31$ s and a transient due to the adaptation of the gains k_1 and k_2 is observed that allows the lift to reach the targeted reference (see Figure 7(a)). The control allows to efficiently track the lift reference despite the perturbation via the averaged duty-cycle (Figure 7(c)): the gains k_1 and k_2 (see Figure 7(b)) quickly increase to compensate the lower value of the lift due to the perturbation. The effort requested to maintain the tracking efficiency depends on the reference and the perturbation; as a consequence, a lower reference at $t = 63$ s tends to decrease the gains k_1 and k_2 despite the constant perturbation (see Figures 7(a) and 7(b)).

- **Scenario 2:** Figure 8 illustrates the tracking of the lift considering piece-wisely constant modifications of the reference under a change of the wind speed (maintained during the rest of the scenario) as well as the introduction of a chopper perturbation while the control is running. The wind speed is initially set to 20.3 ms^{-1} and no perturbation is introduced at the initial time. The wind speed is set at 21.3 ms^{-1} at $t = 12$ s until the end of the scenario. The gains are adapting themselves according to this lift increase, with a relatively long time transient of gains until $t = 25$ s (Figure 8(b)). Accordingly, the reaction of the control can be seen both through the value of the averaged duty-cycle (Figure 8(c)) that is adjusted when perturbations occur and through the adaptation of k_1 and k_2 (Figure 8(b)) that are increased while the perturbations occur. Another perturbation is introduced by moving the chopper blade into the inlet of the test section at $t = 50$ s. This perturbation isn't strong enough to induce a control reaction. It is increased further by introducing the chopper blade further into the inlet at $t = 60$ s. As soon as this perturbation is introduced, the control reacts strongly by increasing gains k_1 and k_2 (see figure 8 (b)). Lastly, a new reference is imposed at a lower lift level which allows a greater controlability margin of the actuator, then the gains k_1 and k_2 can be increased to cope with the chopper perturbation. According to the adaptation rules, the gains are dynamically increased while a perturbation is disturbing the lift (either the wind speed or the static chopper) to compensate the perturbation and to maintain the tracking. When starting the control, a certain transient is needed to start the adaptation of the gain to set the initial tracking of the lift (see Figures 8(b) and 8(b)).

Scenario 3: Figure 9 illustrates the tracking of a sine reference at a constant wind speed of 20.3 ms^{-1} is considered and without chopper perturbation. The gains update quickly (at 10 s for k_1 and at 20 s for k_2) and reach higher values before oscillating according to the reference and the rejection of the aerodynamic fluctuations. In particular, some strong aerodynamic fluctuations occur when the reference becomes higher, thus disturbing the tracking, around the maximum of the lift, that is rapidly compensated by the adjustment of the gains. The high frequency variations of the duty-cycle (Figure 9(c)) are probably due to the effect of the binary valves on the closed-loop control. Moreover, the two bumps which appear on k_1 and k_2 are due to the highest reference variation in absolute value.

Scenarios including saturation while starting the control:

- **Scenario 4:** Figure 10 illustrates the tracking of a constant reference and wind speed of 20.3 ms^{-1} considering an initial saturation of the control, and the introduction of the chopper at $t = 30$ s. During the saturation, the gains k_1 and k_2 are maintained constant and the control reacts after the saturation period with a small delay. The oscillations (or chattering) present in the duty-cycle is in relation with the value of the gains. Particularly, the chattering is reduced when the gains are the lowest at around 35 s; this is again certainly related to the binary valves.

- **Scenario 5:** Figure 11 illustrates the tracking of the lift considering an initial saturation of the control, piece-wisely constant changes of the reference as well as the introduction of the chopper perturbation during the control. The saturation of the control is again reached at the beginning and the chopper is introduced at $t = 30$ s, similarly as scenario 4, except that changes of the reference are considered. The gains k_1 and k_2 are stabilized until $t = 50$ s despite the chopper perturbation that is introduced at $t = 30$ s. The changes of the reference impact the adjustment of the gains k_1 and k_2 for which the gains are strongly reduced when the lift reference is set at the lowest value. Notice that, when the lift reference is set again at its nominal value at $t = 90$ s, the adaptation of the gains takes more time when re-increasing the lift reference, which induces a slower transient.
  When the reference is lower, the control is relaxed involving a fast return of the initial state of the flow (separated flow). At the opposite, more energy is needed to force the flow attachment, inducing an increase of the gains k_1 and k_2. This last operation takes more time by the control (see the time evolution of the gains k_1 and k_2 in Figure 11(c)). This is in good agreement with the study of [11] who found a faster return to the initial state (flow separation) when the control is removed.

- **Scenario 6:** Figure 12 illustrates the tracking of the lift considering an initial saturation of the control, piece-wisely constant changes of the reference as well as the introduction of a short-time stronger static chopper perturbation, introduced at $t = 30$ s and removed at $t = 80$ s. The wind speed is set at a constant speed of 20.3 ms^{-1}. This case shows higher aerodynamic perturbations when introducing the chopper, while the control maintains good tracking response. Compared to the previous case, the gains evolves in the same way before the removal of the chopper, but the adaptation of the gains from $t = 80$ s is faster since the chopper has been removed which tends to indicate that the control efficiency is decreased by the chopper perturbation (more turbulence).

- **Scenario 7:** Figure 13 illustrates the tracking of the lift considering piece-wisely constant changes of the reference under a lower wind speed of 19.3 ms^{-1} (lower Reynolds number because the blade section is the same), no external perturbations have been introduced. Globally, due to the low wind speed, less effort is made to maintain the lift despite the changes of the reference. In particular, the gains remain low in average and a reduction of the perturbations is observed at the lowest lift reference that can be correlated with corresponding low gains values and the decrease of the duty-cycle. The chattering effect is then of less importance, in agreement with reduced gains used in this configuration and thus less perturbations from the binary valves.

The rejection of the high frequency perturbations can be managed differently considering another choice of β, ϵ, k_1 and k_2 in equations (4) and (5). The high frequency perturbations are, to the best of knowledge, also due to the limitations of the dynamic of the micro-jets and measurement noise.

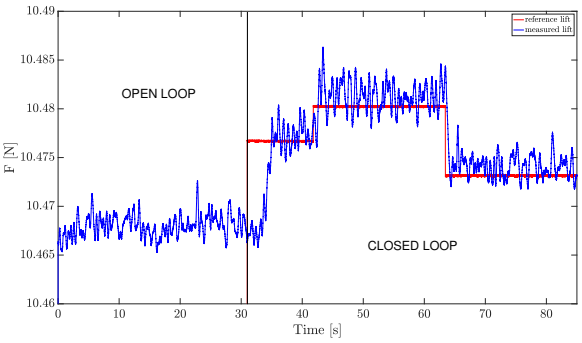

(a) Measured lift and reference lift versus time (sec).

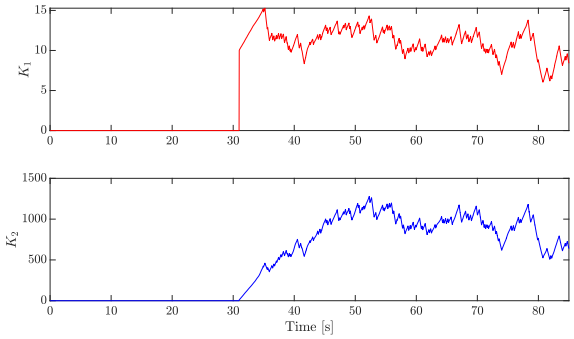

(b) Gains k_1 and k_2 versus time (sec).

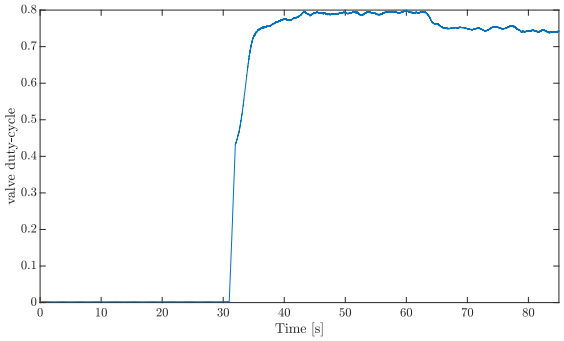

(c) Duty-cycle versus time (sec).

Fig. 7: Scenario 1: open-loop, chopper perturbation while starting the control.

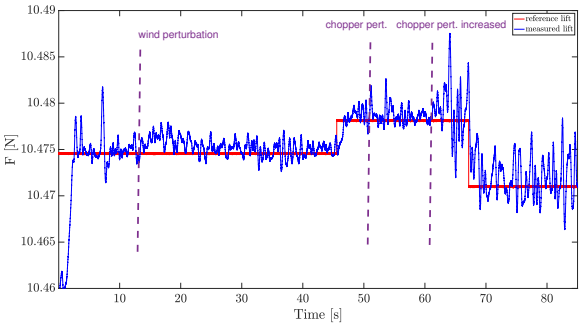

(a) Measured lift and reference lift versus time (sec).

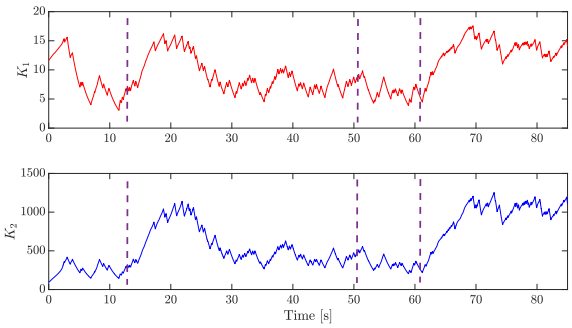

(b) Gains k_1 and k_2 versus time (sec).

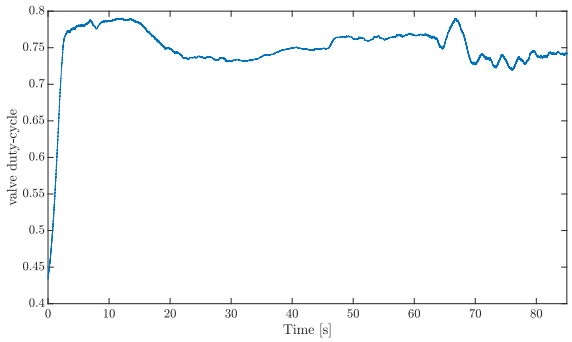

(c) Duty-cycle versus time (sec).

Fig. 8: Scenario 2: wind speed change (+ $\mathbf{1}\mathrm{ms}^{-1}$) and chopper perturbations during the control.

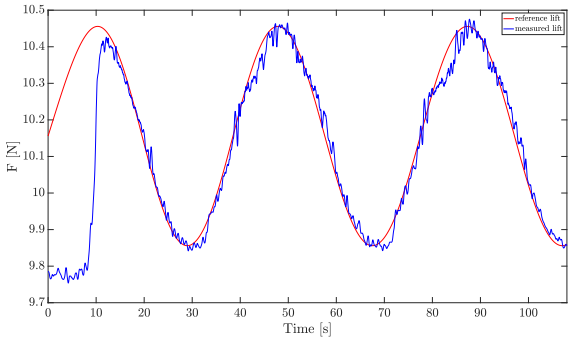

(a) Measured lift and reference lift versus time (sec).

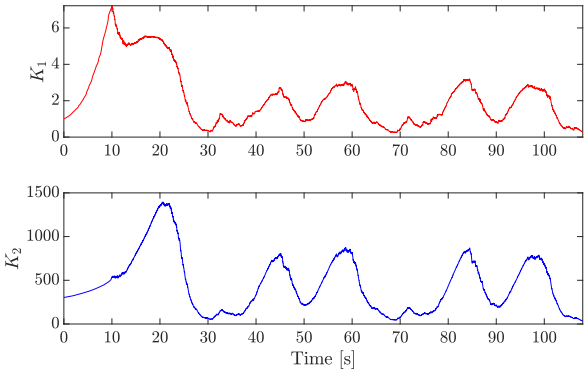

(b) Gains k_1 and k_2 versus time (sec).

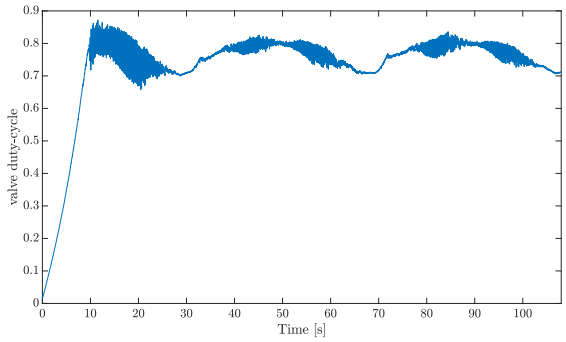

(c) Duty-cycle versus time (sec).

Fig. 9: Scenario 3: oscillating reference without any perturbation.

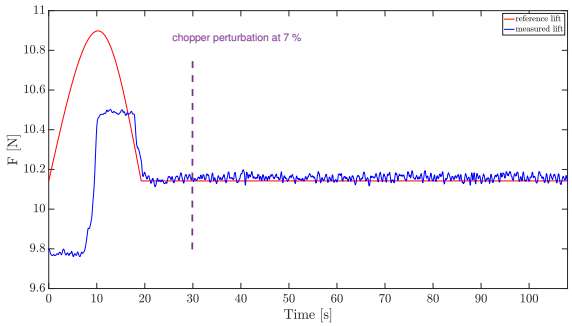

(a) Measured lift and reference lift versus time (sec).

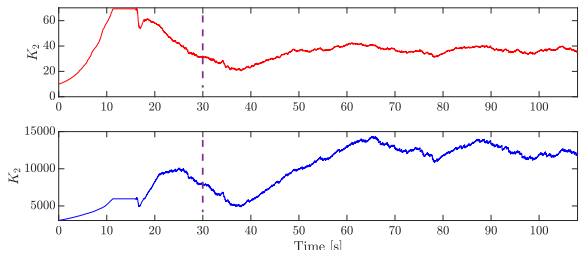

(b) Gains k_1 and k_2 versus time (sec).

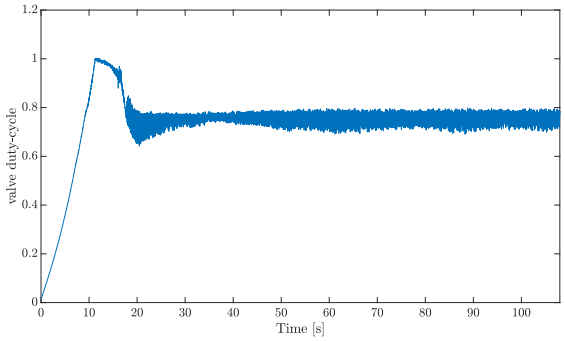

(c) Duty-cycle versus time (sec).

Fig. 10: Scenario 4: constant reference and chopper perturbation during the control.

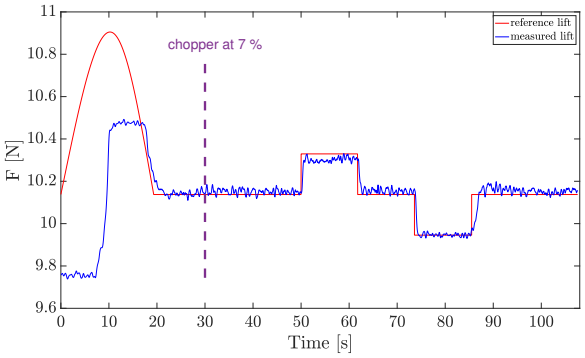

(a) Measured lift and reference lift versus time (sec).

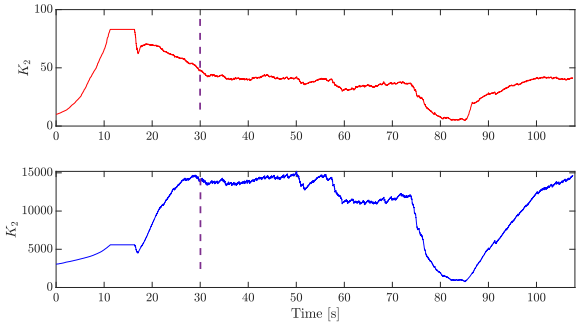

(b) Gains k_1 and k_2 versus time (sec).

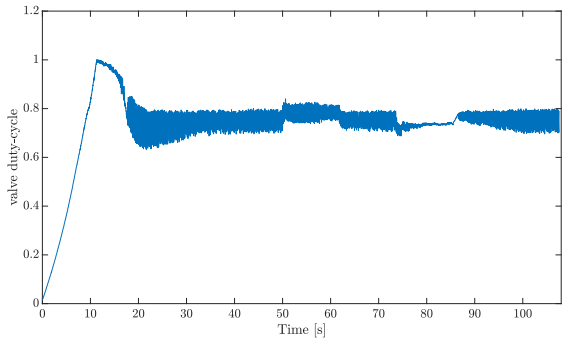

(c) Duty-cycle versus time (sec).

Fig. 11: Scenario 5: chopper perturbation during the control.

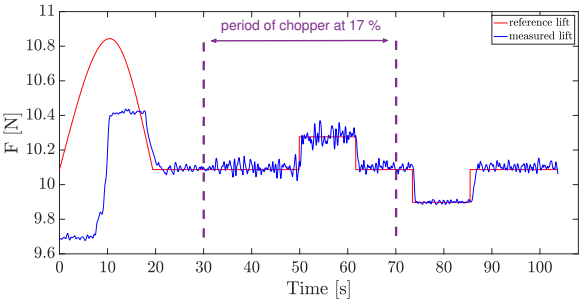

(a) Measured lift and reference lift versus time (sec).

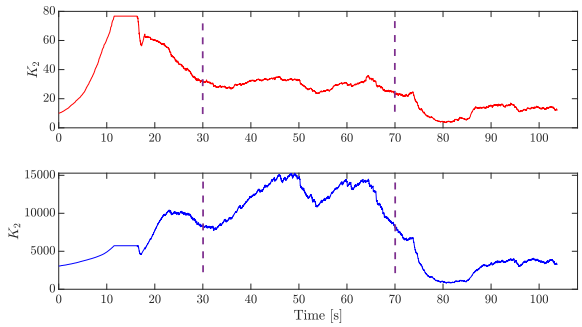

(b) Gains k_1 and k_2 versus time (sec).

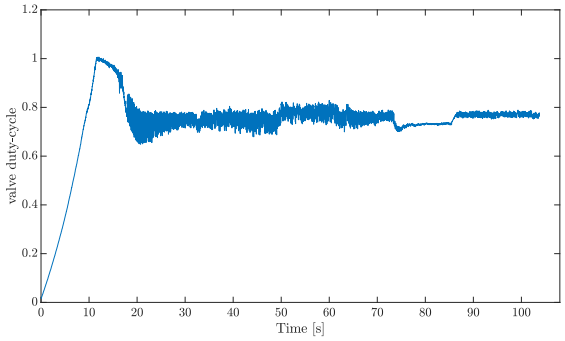

(c) Duty-cycle versus time (sec).

Fig. 12: Scenario 6: short-time chopper perturbation during the control.

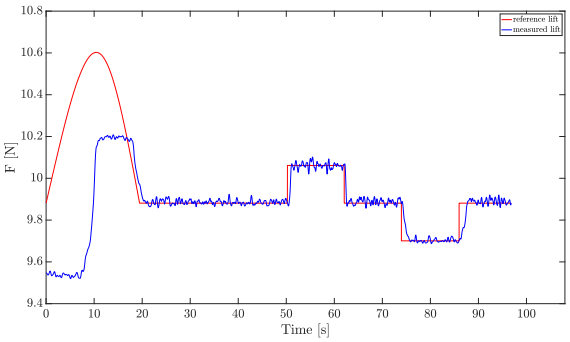

(a) Measured lift and reference lift versus time (sec).

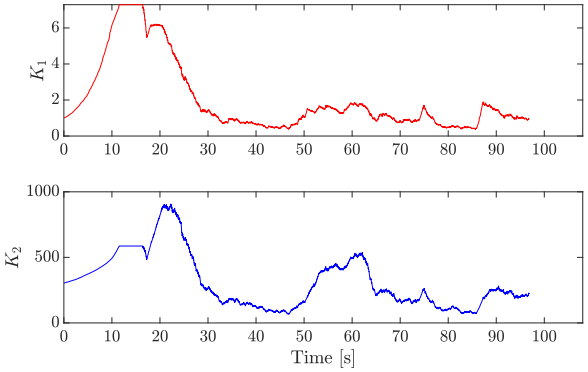

(b) Gains k_1 and k_2 versus time (sec).

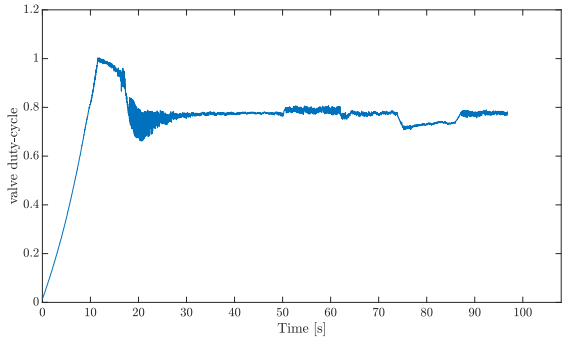

(c) Duty-cycle versus time (sec).

Fig. 13: Scenario 7: lower wind speed ($19.3\,\mathrm{ms}^{-1}$).

V. Conclusion

An adaptive super-twisting-based control has been used to control the lift force acting on an airfoil by means of micro-jets. Different scenarios of experimental tests have been carried out to illustrate the robustness of the control. Promising results show that satisfying tracking performances have been obtained despite the perturbations made of two types: chopper blade perturbation which is increasing the turbulence intensity level of the inflow, and mean wind inflow variations.

Due to the small range of the lift controlability, the micro-jet action is rather limited. The anti-windup manages the saturation of the control efficiency. To extend the capabilities of the proposed lift control system, the direct control of the angle of attack is envisaged and future investigations will be focused on the lift control design combining the use of blade pitch and the use of micro-jets.

To summarize the results obtained with the test-bed:

- the proposed control is robust to saturation and to external perturbations;
- the control needs more energy when the chopper appears (in the considered cases) than when the tracking reference changes;
- the adaption of the control takes time with respect to wind perturbation.

In order to overcome the chattering due to the binary valves, continuous valves could be tested in the future. Moreover, a spatio-temporal measurement should be used to investigate complex fluidic organisation in closed-loop compared with open-loop behavior.

Acknowledgments

The authors thank Dr. Pierre Molinaro for the design of the electronic control board in the experimental setup. This work is supported by *Agence Nationale de la Recherche* (ANR) with project CREATIF ANR-20-CE05-0039. and ASAPe Pays-de-la-Loire regional project (grant no. 2018 ASAPe).

References

[1] J. Schepers *et al.*, IEA Wind TCP Task 29, Phase IV: Detailed Aerodynamics of Wind Turbines, Tech. Rep., may 2021.

[2] E. Bossanyi, "The design of closed loop controllers for wind turbines," *Wind Energy*, vol. 3, pp. 149–163, 2000.

[3] A. Gomez Gonzalez, P. B. Enevoldsen, A. Barlas, and H. A. Madsen, "Field test of an active flap system on a full-scale wind turbine," *Wind Energy Science*, vol. 6, no. 1, pp. 33–43, 2021.

[4] A. M. Cooperman and C. P. van Dam, "Closed-loop control of a microtab-based load control system," *Journal of Aircraft*, vol. 52, no. 2, pp. 387–394, 2015.

[5] H. Matsuda, M. Tanaka, T. Osako, K. Yamazaki, N. Shimura1, M. Asayama, and Y. Oryu, "Plasma actuation effect on a mw class wind turbine," *International Journal of Gas Turbine, Propulsion and Power Systems*, vol. 9, no. 1, 2017.

[6] D. R. Williams and R. King, "Alleviating unsteady aerodynamic loads with closed-loop flow control," *AIAA Journal*, vol. 56, no. 6, pp. 2194–2207, 2018.

[7] B. G. Allan, J. Juang, D. L. Raney, A. Seifert, L. G. Pack, and D. E. Brown, "Closed-loop separation control using oscillatory flow excitation," NASA/CR-2000-210324, ICASE Report 2000-32, Tech. Rep., 2000.

[8] N. Li and M. J. Balas, "Aeroelastic control of wind turbine blade using trailing-edge flap," *Wind Engineering*, vol. 38, no. 5, pp. 549–560, 2014.

[9] S. Bartholomay *et al.*, "Pressure-based lift estimation and its application to feedforward load control employing trailing-edge flaps," *Wind Energy Science*, vol. 6, no. 1, pp. 221–245, 2021.

[10] T. Barlas, J. W. van Wingerden, A. Hulskamp, and G. van Kuik, "Closed-loop control wind tunnel tests on an adaptive wind turbine blade for load reduction," in *46th AIAA Aerospace Sciences Meeting and Exhibit*, 2008.

[11] T. Shaqarin, C. Braud, and S. Coudert, "Open and closed-loop experiments to identify the separated flow dynamics of a thick tbl," *Experiment in fluids*, vol. 54, no. 1448, 2013.

[12] N. Li and M. J. Balas, "Adaptive flow control of wind turbine blade using microtabs with unsteady aerodynamic loads," in *2013 IEEE Green Technologies Conference (GreenTech)*, 2013, pp. 134–139.

[13] T. Shaqarin, "Active control to reattach a thick turbulent boundary layer," Ph.D. dissertation, Ecole Centrale Lille, France, Nov. 2011.

[14] R. Becker, M. Garwon, C. Gutknecht, G. Barwolf, and R. King, "Robust control of separated shear flows in simulation and experiment," *J. of Process Control*, vol. 15, pp. 691–700, 2005.

[15] V. Jaunet and C. Braud, "Experiments on lift dynamics and feedback control of a wind turbine blade section," *Renewable Energy*, vol. 126, pp. 65–78, 2018.

[16] S. Aubrun, A. Leroy, and P. Devinant, "A review of wind turbine-oriented active flow control strategies," *Experiments in Fluids*, vol. 58, 09 2017.

[17] M. Fliess and C. Join, "Model-free control," *International Journal of Control*, vol. 86, no. 12, pp. 2228–2252, 2013.

[18] L. Michel, I. Neunaber, R. Mishra, C. Braud, F. Plestan, J.-P. Barbot, X. Boucher, C. Join, and M. Fliess, "Model-free control of the dynamic lift of a wind turbine blade section: experimental results," *Journal of Physics: Conference Series*, vol. 2265, no. 3, p. 032068, May 2022. [Online]. Available: https://hal.archives-ouvertes.fr/hal-03787439

[19] S. Brunton and B. Noack, "Closed-loop turbulence control: Progress and challenges," *Applied Mechanics Reviews*, vol. 67, 07 2015.

[20] Y. Shtessel, C. Edwards, L. Fridman, and A. Levant, *Sliding Mode Control and Observation*. Springer, New York, USA, 2014.

[21] V. Utkin and H.-C. Chang, "Sliding mode control on electro-mechanical systems," *Mathematical Problems in Engineering*, vol. 8, 2002.

[22] B. Draženović, "The invariance conditions in variable structure systems," *Automatica*, vol. 5, no. 3, pp. 287–295, 1969.

[23] K. Mariette, "Contrôle en boucle fermée pour la réduction active de traînée aérodynamique des véhicules," Ph.D. dissertation, INSA of Lyon, France., Nov. 2020.

[24] R. Becker, R. King, R. Petz, and W. Nitsche, "Adative closed-loop separation control on a high-lift configuration using extremum seeking," *AIAA Journal*, vol. 45, no. 6, pp. 1382–1392, 2007.

[25] A. Levant, "Sliding order and sliding accuracy in sliding mode control," *International Journal of Control*, vol. 58, no. 6, pp. 1247–1463, 1993.

[26] F. Plestan, Y. Shtessel, V. Brégeault, and A. Poznyak, "New methodologies for adaptive sliding mode control," *International Journal of Control*, vol. 83, no. 9, pp. 1907–1919, 2010.

[27] G. Bartolini, A. Levant, F. Plestan, M. Taleb, and E. Punta, "Adaptation of sliding modes," *IMA Journal of Mathematical Control and Information*, vol. 30, no. 3, pp. 285–300, 2013.

[28] L. Hsu, T. Oliveira, J. Paulo, V. Cunha, and L. Yan, "Adaptive unit vector control of multivariable systems using monitoring functions," *International Journal on Robust and Nonlinear Control*, vol. 29, no. 3, pp. 583–600, 2019.

[29] S. Roy, S. Baldi, and L. Fridman, "On adaptive sliding mode control without a priori bounded uncertainty," *Automatica*, vol. 11, 2020.

[30] L. Lin, Z. Liu, Y. Kao, and R. Xu, "Adaptation of sliding modes," *IET Control Theory & Applications*, vol. 14, no. 3, pp. 519–525, 2020.

[31] H. Obeid, L. Fridman, S. Laghrouche, and M. Harmouche, "Barrier function-based adaptive sliding mode control," *Automatica*, vol. 93, pp. 540–544, 2018.

[32] Y. Shtessel, J. Moreno, and L. Fridman, "Twisting sliding mode control with adaptation: Lyapunov design, methodology and application," *Automatica*, vol. 75, pp. 229–235, 2017.

[33] G. Liu, A. Zinober, Y. Shtessel, and Q. Niu, "Twisting sliding mode control with adaptation: Lyapunov design, methodology and application," *Australian Journal of Electrical and Electronics Engineering*, vol. 9, no. 3, pp. 217–224, 2012.

[34] M. Taleb, A. Levant, and F. Plestan, "Electropneumatic actuator control: solutions based on adaptive twisting algorithm and experimentation," *Control Engineering Practice*, vol. 21, no. 5, pp. 727–736, 2013.

[35] Y. Shtessel, M. Taleb, and F. Plestan, "A novel adaptive-gain supertwisting sliding mode controller: methodology and application," *Automatica*, vol. 48, no. 5, pp. 759–769, 2012.
[36] C. Edwards and Y. Shtessel, "A novel adaptive-gain super-twisting sliding mode controller: methodology and application," *International Journal of Control*, vol. 89, no. 9, pp. 1759–1766, 2016.
[37] V. Utkin and A. Poznyak, "Adaptive sliding mode control with application to super-twist algorithm: Equivalent control method," *Automatica*, vol. 49, no. 1, pp. 39–47, 2013.
[38] H. Obeid, S. Laghrouche, L. Fridman, Y. Chitour, and M. Harmouche, "Barrier function-based adaptive super-twisting controller," *IEEE Transactions on Automatic Control*, vol. 65, no. 11, pp. 4928–4933, 2020.
[39] S. Gutierrez, J. de Léon-Morales, F. Plestan, and A. S. Pena, "A simplified version of adaptive super-twisting control," *International Journal of Robust and Nonlinear Control*, vol. 29, no. 16, pp. 5704–5719, 2019.
[40] F. Plestan and M. Taleb, "Adaptive supertwisting controller with reduced set of parameters," in *2021 European Control Conference (ECC)*, 2021, pp. 2627–2632.
[41] L. Michel, I. Neunaber, R. Mishra, C. Braud, F. Plestan, J.-P. Barbot, and P. Hamon, "A novel lift controller for a wind turbine blade section using an active flow control device: experimental results," in *The IEEE 2022 Conference on Control Technology and Applications (CCTA)*. Trieste, Italy: to appear, Aug. 2022. [Online]. Available: https://hal.archives-ouvertes.fr/hal-03787452
[42] A. Soulier, C. Braud, D. Voisin, and B. Podvin, "Low-Reynolds-number investigations on the ability of the strip of tell-tale sensor to detect flow features over wind turbine blades: flow separation/reattachment dynamics," *Wind Energy Science*, vol. 6, pp. 409–426, 2021.
[43] E. Hairer, S. Nørsett, and G. Wanner, *Solving Ordinary Differential Equations I Nonstiff problems*, 2nd ed. Berlin: Springer, 2000.
[44] M. Fliess, C. Join, and H. Sira-Ramirez, "Non-linear estimation is easy," *International Journal of Modelling, Identification and Control*, vol. 4, no. 1, pp. 12–27, 2008.
[45] L. Michel, S. Selvarajan, M. Ghanes, F. Plestan, Y. Aoustin, and J.-P. Barbot, "An experimental investigation of discretized homogeneous differentiators: Pneumatic actuator case," *IEEE Journal of Emerging and Selected Topics in Industrial Electronics*, vol. 2, no. 3, pp. 227–236, 2021.
[46] A. Othmane, J. Rudolph, and H. Mounier, "Systematic comparison of numerical differentiators and an application to model-free control," *European Journal of Control*, vol. 62, pp. 113–119, 2021.
[47] J.-P. Barbot, A. Levant, M. Livne, and D. Lunz, "Discrete differentiators based on sliding modes," *Automatica*, vol. 112, p. 108633, 2020.
[48] M. Ghanes, J. P. Barbot, L. Fridman, A. Levant, and R. Boisliveau, "A new varying gain exponent based differentiator/observer: an efficient balance between linear and sliding-mode algorithms," *IEEE Trans. on Automatic Control*, 2020.
[49] S. Tarbouriech, G. Garcia, J. Silva, and I. Queinnec, *Stability and Stabilization of Linear Systems with Saturating Actuators*, 01 2011.

Loïc Michel is currently postdoctoral fellow at the Ecole Centrale de Nantes, France, working on advanced homogeneous control and differentiation techniques. He received his Ph.D. in electrical engineering in 2012 from the University of Quebec, Canada. His research interests include advanced techniques for robust and intelligent control with applications in biology, mechatronic systems, aerodynamics and neural networks.

Ingrid Neunaber is a postdoctoral fellow at the Norwegian University of Science and Technology, Norway, who previously worked for the CNRS at the LHEEA laboratory at Centrale Nantes, France, as a postdoctoral researcher. She received her Ph.D. in 2019 in experimental wind energy physics from the University of Oldenburg. Her research interests include turbulence, wind energy, wakes, and aerodynamics.

Rishabh Mishra is a PhD candidate at the LHEEA laboratory of CNRS and École Centrale de Nantes working on turbulent inflow customisation. He received his MS in Hydrodynamics from Ecole Centrale de Nantes, B.Tech. in Naval Architecture and Ocean Engineering and B.Sc. in Ship Building and Repair from Indian Maritime University. His research interests include theoretical, experimental and numerical analysis of turbulent flow fields.

Caroline Braud is a senior CNRS researcher. She received her Ph.D. in Fluid Dynamics in 2003 from Poitiers University, France. She then worked two years as an associate researcher at Syracuse University, USA, NY state. She joined the CNRS in 2005 and was assigned to the LMFL laboratory in Lille, France. She moved to the LHEEA laboratory from Ecole Centrale Nantes in 2015 to work on Wind Energy. Since 2021 she shares her time between the LHEEA laboratory and CSTB-Nantes in France, where she is in charge of the wind energy research development. Her research interests include turbulent shear flows, unsteady aerodynamics, wind tunnel experiments, flow control experiments (AFC: Active Flow Control), wind turbine field tests and wind turbine blade monitoring and control.

Franck Plestan received the Ph.D. in Automatic Control from the Ecole Centrale de Nantes, France, in 1995. From September 1996 to August 2000, he was with Louis Pasteur University, Strasbourg, France. In September 2000, he joined the Ecole Centrale de Nantes, Nantes, France where he is currently Professor. His research interests include robust nonlinear control and estimation (higher order sliding mode, time delay), and applications (pneumatic actuator, robotics, wind turbine).

Preprint submitted to IEEE Transactions on Control Systems Technology. Received: November 30, 2022 11:18:28 Pacific Time

Jean-Pierre Barbot is Professor at ENSEA Cergy-Pontoise, France and he is actually in secondment at LS2N-CNRS Nantes. He was the former director of the Quartz Laboratory EA 7393 and former member of EPI Non-A at INRIA. After his graduation from the *Ecole Normale Supérieure of Cachan* (France), he received the Ph. D. degree in automatic control from the University of Paris XI (France) in 1989 and the HDR in 1997. These main research activities deal with sliding mode control and observation, system under sampling, hybrid system, delay system, synchronization of chaotic system, normal form and recently sparsity apply to FDI and Cyber-attack detection. These main application domains are electrical machine, power converter and renewable energy.

Pol Hamon received the M.S. degree in robotics and control from the Institut National des Sciences Appliquées, Rennes, France, in 2018. He is curently working toward the Ph.D degree in robotics and control engineering at the Ecole Centrale de Nantes, France. His resarch is focused on robotics hand and model-free control.